第 35 卷第 11 期
2019 年 11 月

无 机 化 学 学 报
CHINESE JOURNAL OF INORGANIC CHEMISTRY

Vol.35 No.11
2159-2167

3,3′-(吡啶-3,5)二苯甲酸构筑的 Co(Ⅱ)/Ni(Ⅱ)配合物的合成、晶体结构及性质

韩 晓[1,2] 邵志超[2] 赵 蓓[2] 任 宁[1] 孟祥茹[2] 丁 洁[2] 侯红卫*[,2]

([1]邯郸学院化学化工与材料学院,邯郸 056000)

([2]郑州大学化学与分子工程学院,郑州 450001)

摘要:设计、合成了 2 个配合物:{[Co_2(pddb)$_2$(μ_2-H_2O)(H_2O)$_2$]·2DMA·5H_2O}$_n$ (**1**)和{[Ni_2(pddb)$_2$(μ_2-H_2O)(H_2O)$_2$]·2DMA·5H_2O}$_n$ (**2**)(H_2pddb=3,3′-(吡啶-3,5)二苯甲酸,DMA=*N*,*N*-二甲基乙酰胺),并通过红外光谱(IR),元素分析,热重分析(TG)和单晶 X 射线衍射确定它们的结构。结构分析表明 **1** 和 **2** 是异质同构的,其空间构型可简化成(3,6)连接的拓扑结构,其符号为(4^2·6)·(4^4·6^2·8^8·10)。进一步研究了配合物 **1** 和 **2** 的固体紫外、磁性及其催化性能。研究表明 **1** 和 **2** 中的中心金属离子之间存在反铁磁耦合作用,并且 **1** 可以作为 C-H 活化的高效非均相催化剂。

关键词:3,3′-(吡啶-3,5)二苯甲酸;配合物;晶体结构;磁性;非均相催化

中图分类号:O614.81$^+$3;O614.81$^+$2 **文献标识码**:A **文章编号**:1001-4861(2019)11-2159-09

DOI:10.11862/CJIC.2019.241

Synthesis, Crystal Structure, Magnetic Properties and Catalytic Activity of Co(Ⅱ)/Ni(Ⅱ) Complexes with 3,3′-(Pyridine-3,5-diyl) Dibenzoic Acid

HAN Xiao[1,2] SHAO Zhichao[2] ZHAO Bei[2] REN Ning[1]

MENG Xiang-Ru[2] DING Jie[2] HOU Hong-Wei*[,2]

([1]*Hebei Key Laboratory of Heterocyclic Compounds, College of Chemical engineering & Material, Handan University, Handan, Hebei* 056005, *China*)

([2]*College of Chemistry and Molecular Engineering, Zhengzhou University, Zhengzhou* 450001, *China*)

Abstract: Two complexes **1**~**2** (**1**={[Co_2(pddb)$_2$(μ_2-H_2O)(H_2O)$_2$]·2DMA·5H_2O}$_n$ and **2**={[Ni_2(pddb)$_2$(μ_2-H_2O)(H_2O)$_2$]·2DMA·5H_2O}$_n$, H_2pddb=3,3′-(pyridine-3,5-diyl) dibenzoic acid, DMA=*N*,*N*-dimethylacetamide) have been synthesized and identified by Infrared spectroscopy (IR), elemental analysis, thermogravimetric analysis (TG) and single crystal X-ray diffraction. Structural analyses show that **1** and **2** are isostructural, and display a 3D (3,6)-connected net with the point symbol (4^2·6)·(4^4·6^2·8^8·10). Besides, the UV-Vis absorption spectra in solid state, the magnetic properties and catalytic activity of **1**~**2** were investigated. Between the proximal Co(Ⅱ)/Ni(Ⅱ) ions, the variable-temperature (2~300 K) magnetic susceptibilities of **1**~**2** display antiferromagnetic coupling. Furthermore, **1** have been verified to be effectual catalysts for the oxidation of arylacycloalkanes in aqueous medium. CCDC: 1952526, **1**; 1952527, **2**.

Keywords: 3,3′-(pyridine-3,5-diyl) dibenzoic acid; complex; crystal structure; magnetic property; heterogeneous catalyst

收稿日期:2019-09-11。收修改稿日期:2019-10-02。

国家自然科学基金(No.21671174,21803016),中原千人计划,河北省高等学校科学技术研究重点项目(No.ZD2019309)和邯郸学院“育苗工程”(2018305)资助。

*通信联系人。E-mail:houhongw@zzu.edu.cn

0 Introduction

Complexes as one of the most attractively versatile platforms for achieving long-range organization and order as well as exploitable property, has been attractive in different areas during the past decade. Due to the adjustable flexibility and connectivity information of ligands, the judicious selection of organic ligands to coordinate with suitable metal centers is a key factor for the modulation of the structure and property of complex. Among this, a variety of complexes have been prepared under hydrothermal conditions by using unsymmetrical N-heterocyclic ligands and aromatic polycarboxylate ligands[1-4], which were favorable for the potential applications in gas adsorption, fluorescence sensing, catalysis and photocatalysis, and molecular switch[5-9]. Bifunctional pridine-carboxylate ligands possess N- and O- potential electron-donating centers which can exhibit diverse coordination modes with metal centers and various structures[10-13]. Notably, carboxylate groups on the ligands may facilitate the formation of discrete multinuclear clusters and infinite building blocks by (M-COO-M) linkage, such as Co(Ⅱ)/Ni(Ⅱ) complexes[14]. It is a crucial way to impart cluster-based complexes with expected magnetic properties and catalysts.

From the reported references, the study of complexes-based heterogeneous catalysts is concentrated on the relation between the structures of heterogeneous catalysts and the size of reaction substrates[15-20]. The influence of central metals to catalytic behaviors has not been systematically researched and discussed[21-24]. It has been observed that the catalytic performance of complexes-based heterogeneous catalysts is strongly dependent on the metal entities[25]. To gain a deep understanding of the relationships between the metal ions and the catalytic behaviors, synthesis and research of isostructural complexes can exclude the influence of ligands and geometries.

Herein, 3,3′-(pyridine-3,5-diyl) dibenzoic acid (H_2pddb) was selected as the organic linker with abundant N-donor sites and two carboxyl groups, which might be partially or completely deprotonated. Through the coordination reactions of $Co(NO_3)_2\cdot 6H_2O$ or $Ni(NO_3)_2\cdot 6H_2O$ with H_2pddb, two isostructural complexes $\{[Co_2(pddb)_2(\mu_2\text{-}H_2O)(H_2O)_2]\cdot 2DMA\cdot 5H_2O\}_n$ (**1**) and $\{[Ni_2(pddb)_2(\mu_2\text{-}H_2O)(H_2O)_2]\cdot 2DMA\cdot 5H_2O\}_n$ (**2**) were obtained, which were identified by elemental analyses, IR, TG, single-crystal X-ray diffractions. In addition, for these complexes, the solid state absorption spectra, magnetic properties and catalytic activity have been investigated.

1 Experimental

1.1 General information and materials

3,3′-(pyridine-3,5-diyl) dibenzoic acid, other reagents and solvents employed were of AR grade from commercial sources and used as received. IR data were recorded on a BRUKER TENSOR 27 spectrophotometer with KBr pellets from 400 to 4 000 cm^{-1}. Elemental analyses (C, H, and N) were carried out on a FLASH EA 1112 elemental analyzer. Powder X-ray diffraction (PXRD) patterns were recorded on a PANalytical X′Pert PRO diffractometer with Cu $K\alpha$ (λ=0.154 18 nm) radiation at room temperature, using an operating tube voltage of 40 kV and tube current of 40 mA in a 2θ range between 5° and 50°. UV-Vis absorption spectra were obtained from Hewlett Packard 8453 UV-Vis Spectrophotometer. Dynamic magnetization experiments of polycrystalline samples were carried out with a SQUID MPMS XL-7 instrument at H=1 000 Oe over a temperature range of 2~300 K. NMR spectra were recorded on 400 MHz Bruker Avance-400 spectrometer and the chemical shift was reported relative to the signals of an internal standard of TMS (δ=0.0).

1.2 Synthesis of complexes

1.2.1 Synthesis of $\{[Co_2(pddb)_2(\mu_2\text{-}H_2O)(H_2O)_2]\cdot 2DMA\cdot 5H_2O\}_n$ (**1**)

A mixture of 3,3′-(pyridine-3,5-diyl) dibenzoic acid (0.009 6 g, 0.03 mmol), $Co(NO_3)_2\cdot 6H_2O$ (0.023 3 g, 0.08 mmol), H_2O (3 mL), and DMA (3 mL) was poured into a vial of PTFE gasket (10 mL), then the vessel was sealed and heated to 100 ℃ for 3 days. The vial was cooled to room temperature at 5 ℃·h^{-1}. Crystals of **1** suitable for X-ray analysis were collected.

Anal. Calcd. for $C_{46}H_{56}Co_2N_4O_{18}$(%): C, 51.55; H, 5.23; N, 5.23. Found(%):C, 50.98; H, 5.36; N, 5.02. IR (KBr, cm^{-1}): 3 431 (w), 3 126 (w), 2 991 (w), 1 703 (w), 1 665 (m), 1 564 (s), 1 432 (m), 1 321 (s), 1 264 (w), 1 108 (w), 982 (w), 755 (m), 557 (w).

1.2.2 Synthesis of $\{[Ni_2(pddb)_2(\mu_2\text{-}H_2O)(H_2O)_2]\cdot 2DMA\cdot 5H_2O\}_n$ (**2**)

A mixture of 3,3′-(pyridine-3,5-diyl) dibenzoic acid (0.009 7 g, 0.03 mmol), $Ni(NO_3)_2\cdot 6H_2O$ (0.023 2 g, 0.08 mmol), H_2O (3 mL), and DMA (3 mL) was poured into a vial of PTFE gasket (10 mL), then the vessel was sealed and heated to 100 ℃ for 3 days. The autoclave was cooled to room temperature at 5 ℃·h^{-1}. Crystals of **2** suitable for X-ray analysis were collected. Anal. Calcd. for $C_{46}H_{56}N_4Ni_2O_{18}$(%):C, 51.57; H, 5.23; N, 5.23. Found(%): C, 51.13; H, 5.46; N, 5.39. IR (KBr, cm^{-1}): 3 418 (w), 3 024 (w), 2 889 (w), 1 698 (w), 1 612 (m), 1 544 (s), 1 419 (m), 1 319 (s), 1 255 (w), 1 106 (w), 998 (w), 769 (m), 541 (w).

1.3 Typical procedure for C-H bond activation of arylacycloalkane to ketones

A mixture of arylacycloalkane (1 mmol), *tert*-butyl hydroperoxide (TBHP) (1.5 mmol), and catalyst (0.05 mmol) in H_2O (2 mL) was ultrasound at room temperature for 4 h in the air. After reaction finished, catalyst was recovered by centrifugation. The residue was extracted with ethyl acetate and H_2O. The organic phases were combined, dried over anhydrous Na_2SO_4, and concentrated in vacuo. The crude product was purified by column chromatography on silica gel with petroleum ether/ethyl acetate (5∶1, *V*/*V*) as eluent to afford product. The ^1H NMR data of pure products were consistent with previous literature report (Supporting information)[26-28].

1.4 Single-crystal structure determination

The crystallographic data were collected on a Bruker D8 VENTURE diffractometer with Mo $K\alpha$ radiation (λ=0.071 073 nm) at 298 K. The integration of the diffraction data and the intensity corrections were performed using the SAINT program[29]. Semiempirical absorption correction was performed using SADABS program[30]. The structures were solved by direct methods and refined with a full matrix least-squares technique based on F^2 with the SHELXL-2016 crystallographic software package[31]. The hydrogen atoms except for those of water molecules were generated geometrically and refined isotropically using the riding model. Crystallographic data and structure processing parameters are summarized in Table 1.

CCDC: 1952526, **1**; 1952527, **2**.

Table 1　Crystal data and structure refinement data of complexes 1~2

Complex	1	2
Formula	$C_{46}H_{56}Co_2N_4O_{18}$	$C_{46}H_{56}N_4Ni_2O_{18}$
Formula weight	1 070.81	1 070.36
Crystal system	Monoclinic	Monoclinic
Space group	*C*2/*c*	*C*2/*c*
a / nm	2.009 7(5)	1.997 8(8)
b / nm	1.100 2(4)	1.094 5(3)
c / nm	2.212 3(6)	2.197 0(5)
β / (°)	92.750(7)	93.146(10)
V / nm^3	4.886(3)	4.797(3)
Z	4	4
D_c / (g·cm^{-3})	1.456	1.482
μ / mm^{-1}	0.757	0.865
2θ range / (°)	4.222~55.054	4.244~55.072
F(000)	2 232.0	2 240.0
Data, restraint, parameter	5 586, 0, 327	5 507, 0, 324
Reflection collected	38 980	37 799
Goodness of fit on F^2	1.057	1.032

Continued Table 1

Final R indices [$I>2\sigma(I)$]	R_1=0.041 5, wR_2=0.113 9	R_1=0.041 7, wR_2=0.108 7
Final R indices (all data)	R_1=0.048 9, wR_2=0.118 9	R_1=0.057 4, wR_2=0.116 9
Largest diff. peak and hole / (e·nm^{-3})	730, −600	560, −610

2 Results and discussion

2.1 Description of the crystal structures

2.1.1 Crystal structure of $\{[Co_2(pddb)_2(\mu_2\text{-}H_2O)(H_2O)_2]\cdot 2DMA\cdot 5H_2O\}_n$ (1)

The X-ray crystallographic analysis reveals that complex **1** crystallizes in the monoclinic space group *C*2/*c*. The asymmetric unit of **1** consists of one Co(Ⅱ) ion, one $pddb^{2-}$ ligand, one coordinated water molecule, one half μ_2-H_2O, two and half lattice-water molecules, and one free DMA molecules. As shown in Fig.1(a), each Co(Ⅱ) ion is six-coordinated with a regular octahedron geometry, which is formed by three oxygen atoms (Co1-O: 0.207 05(16), 0.209 37(16) and 0.210 57(16) nm) from different $pddb^{2-}$ ligands, one nitrogen atom (Co1-N: 0.217 61(18) nm) from one $pddb^{2-}$ ligand, one oxygen atoms (Co1-O: 0.214 09(18) nm) from coordinated water molecule and one μ_2-H_2O (Co1-O: 0.216 03(13) nm).

Two Co(Ⅱ) ions are connected together by one μ_2-H_2O and two carboxylate group from $pddb^{2-}$ to form a second building unit (SBU) of $[Co_2(CO_2)(\mu_2\text{-}H_2O)]$ with a Co⋯Co distance of 0.359 81 nm (Fig.1(b)). The coordination mode of the $pddb^{2-}$ ligand can be described as μ_3-η^1:η^1:η^1 (Fig.1(a)). The dihedral angle between the plane P_1 and plane P_2 is 36.324°, and the dihedral angle between the plane P_2 and plane P_3 is 41.706°. A better insight into the present 3D framework can be accessed by the topological method. As shown in Fig.2 (a), each $[Co_2(CO_2)(\mu_2\text{-}H_2O)]$ SBUs coordinates six

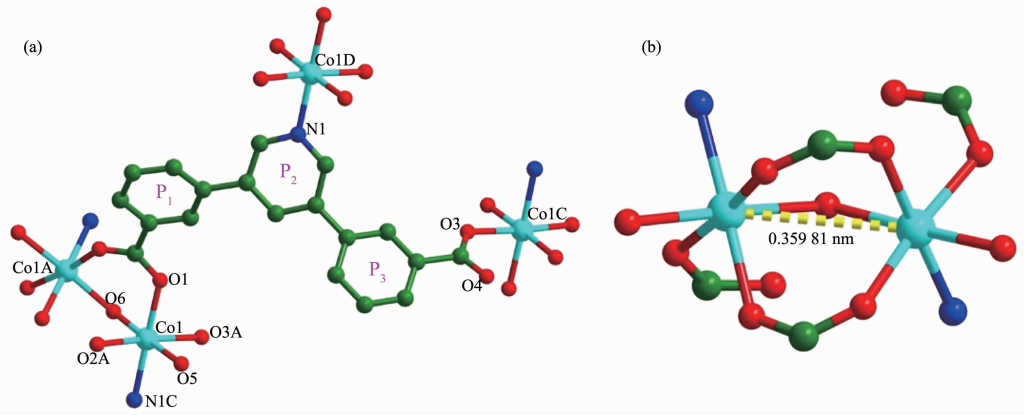

Hydrogen atoms and free solvent molecules are omitted for clarity; Symmetry codes: A: 1−x, +y, 1/2−z; B: 3/2−x, 3/2−y, −z; C: −1/2+x, 1/2+y, +z; D: 1/2+x, −1/2+y, +z

Fig.1 (a) Coordination environments of the Co(Ⅱ) ions in **1**; (b) $[Co_2(CO_2)(\mu_2\text{-}H_2O)]$ SBUs in **1**

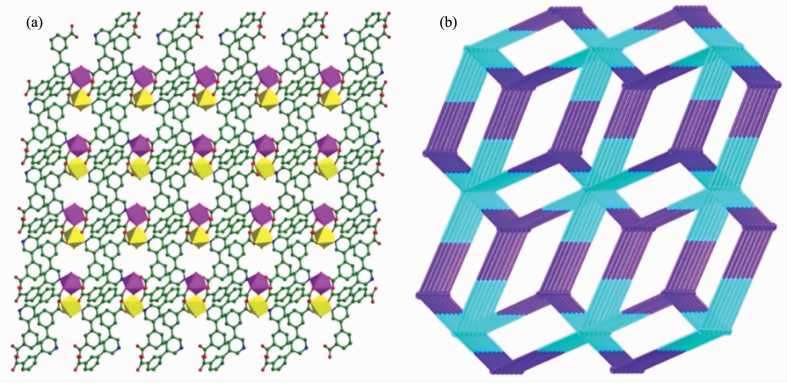

Fig.2 (a) 3D structure of **1** viewed along *a* axis; (b) Topological structure of (3,6)-connected with **1** nodal net

different $pddb^{2-}$ ligands and can be simplified as a 6-connected node, and one $pddb^{2-}$ links three $[Co_2(CO_2)(\mu_2\text{-}H_2O)]$ SBUs, serving as a 3-connected node. Therefore, the structure of complex **1** is a binodal 3,6-connected 3D framework with a point symbol of $(4^2\cdot6)\cdot(4^4\cdot6^2\cdot8^8\cdot10)$, as depicted in Fig.2(b). Finally, 3D supramolecular structure is packed through twelve sorts of hydrogen bonding (classical hydrogen bonding: O–H···O and C–H···O), as shown in Fig.3.

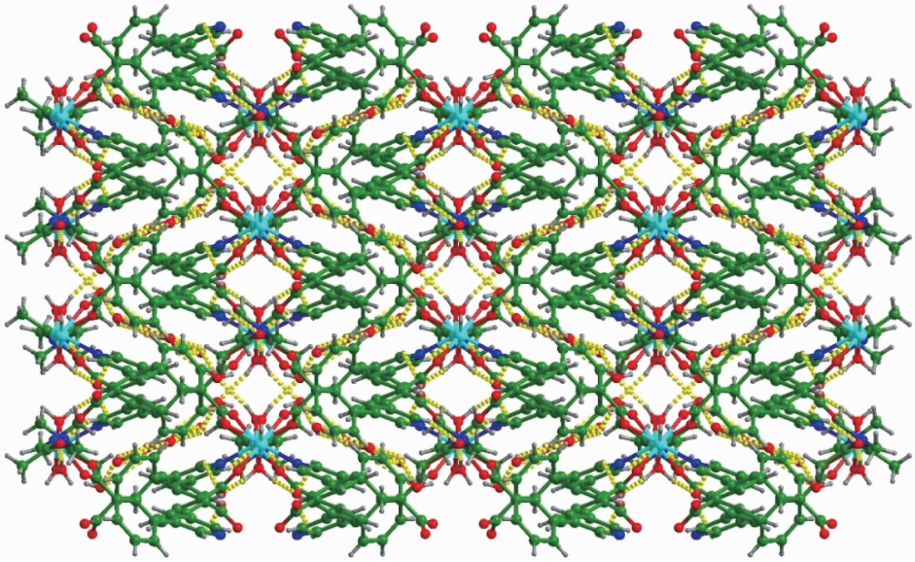

Fig.3 Perspective view of the supramolecular framework through twelve kinds of hydrogen-bonding interactions (dotted line)

2.1.2　Crystal structure of $\{[Ni_2(pddb)_2(\mu_2\text{-}H_2O)(H_2O)_2]\cdot2DMA\cdot5H_2O\}_n$ (**2**)

The single-crystal X-ray diffraction study revealed that **1** and **2** are isostructural and H_2pddb ligands show same coordination mode. Co(Ⅱ) ions in **1** are replaced by Ni(Ⅱ) ions, and there are one free DMA molecule and 2.5 lattice-water molecules in **2** (Fig.4 (a)). Comparing with that of complex **1**, the Ni···Ni distance in the dinuclear unit $[Ni_2(COO)_2(\mu_2\text{-}H_2O)]$ is 0.355 47 nm (Fig.4(b)). The dihedral angle between the planes P_1 and P_2 is 35.824°, and the dihedral angle between the planes P_2 and P_3 is 41.884°. In the crystal structure of **2**, through intramolecular and intermolecular O–H···O and C–H···O hydrogen bonds, adjacent molecules are linked together into 3D supramolecular networks.

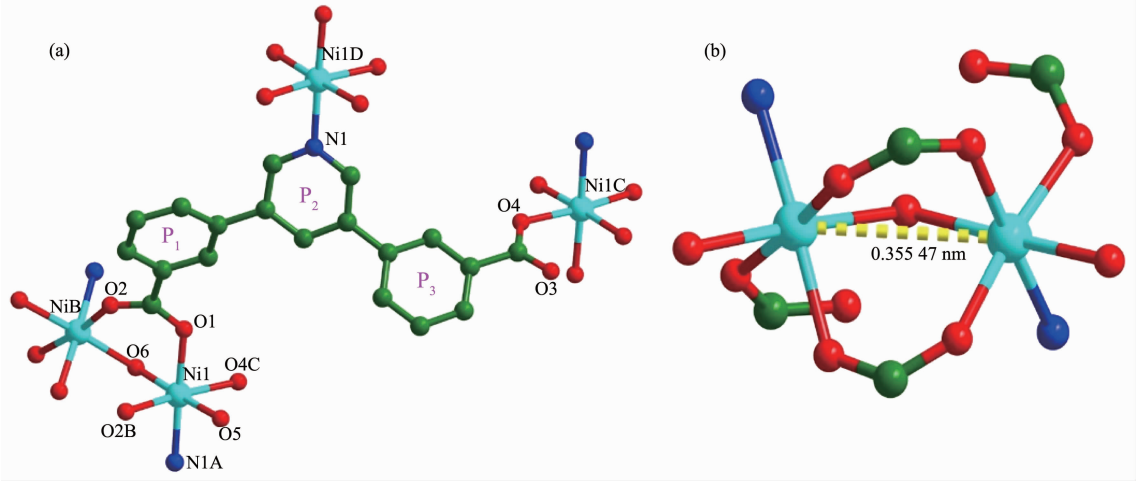

Symmetry codes: A: 1/2+*x*, 1/2+*y*, *z*; B: −*x*, *y*, 1/2−*z*; C: −1/2−*x*, 5/2−*y*, 1−*z*; D: −1/2+*x*, −1/2+*y*, *z*

Fig.4　(a) Coordination environments of the Ni(Ⅱ) ions in **2**; (b) $[Ni_2(CO_2)(\mu_2\text{-}H_2O)]$ SBUs in **2**

2.2 Phase purity and thermogravimetric analysis

To check the phase purity of complexes **1**~**2**, X-ray powder diffraction analyses were checked at room temperature. As shown in Fig.5, the experimental patterns match well with the simulated ones, which manifests the high crystallinity and good phase purities of the samples.

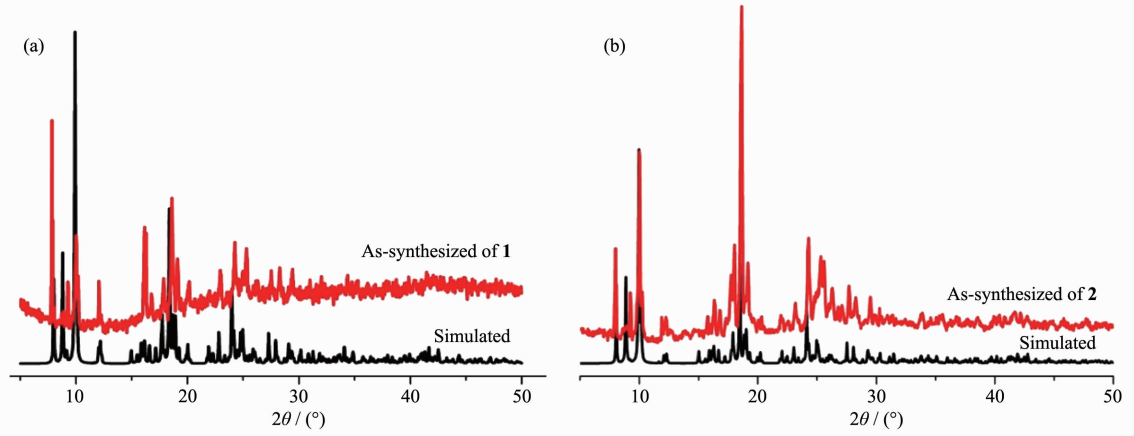

Fig.5 PXRD patterns of the simulated and as-synthesized complexes **1** (a) and **2** (b)

In addition to the phase purity, the thermal properties and the change of crystal forms of **1**~**2** were investigated by using thermogravimetric analysis (TGA) (Fig.6). For complex **1**, the first weight loss was from 30 to 125 ℃ (Obsd. 8.36%, Calcd. 8.41%), corresponding to the removal of the lattice H_2O molecules. The second weight loss of 19.88% (Calcd. 19.64%) corresponds to the loss of free DMA molecule and coordinated water molecules. The removal of μ_2-H_2O and organic ligands occurred within the range of 350~480 ℃, finally leading to the formation of the stoichiometric amount of CoO as a residue. The TG curve for **2** also showed an obvious weight loss between 60 and 350 ℃, which can be ascribed to the removal of lattice water molecules, free DMA molecule and coordinated water molecules (Obsd. 27.41%, Calcd. 28.08%). The removal of organic ligands and μ_2-H_2O occurred within the range of 390~490 ℃. The remaining weight corresponds to the formation of NiO.

2.3 UV-Vis spectra analyses

The solid state absorption spectra of free ligand H_2pddb, **1** and **2** at room temperature were investigated. The electronic absorption spectrum of free ligand H_2pddb exhibited two absorption peaks at approximately 263 and 310 nm. They can be assigned to the π-π^* transition of benzene rings and the intraligand π-π^* transition of the C=N group [32]. The absorption spectra of complexes **1** and **2** were obviously different from those of H_2pddb (Fig.7). In **1**, there are several

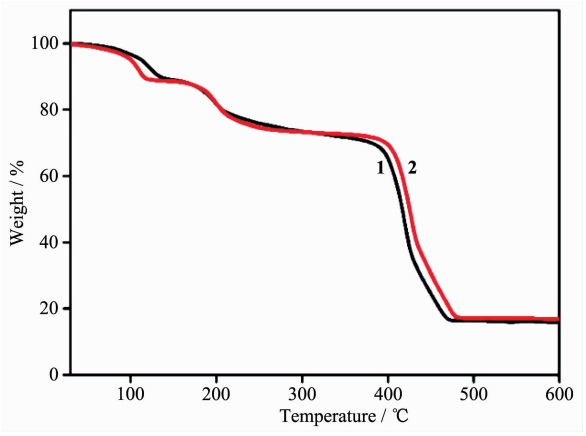

Fig.6 TGA profiles of complexes **1** and **2**

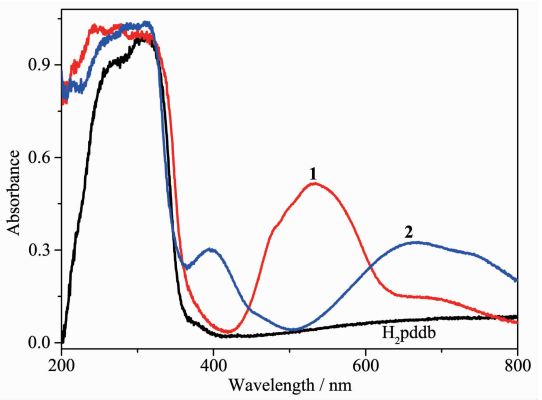

Fig.7 UV-Vis absorption spectra of H_2pddb, **1** and **2** at room temperature

intense absorption bands less than 400 nm and one intermediate absorption band around 535 nm. The absorption band from 200 to 400 nm should be considered as π-π^* transitions of the H_2pddb[33]. Another absorption band from 400 to 700 nm can be ascribed to the spin-allowed *d*-*d* electronic transitions of the d^7 (Co^{2+}) cation[34]. As depicted in Fig.7, the spectra of complex **2** display three wide absorption bands in a range of 200~350 nm, 350~500 nm and 500~800 nm, respectively. The band at 394 and 670 nm are assignable to metal-to-ligand charge transfer (MLCT) transitions ($^3A_{2g}$-$^3T_{1g}$), indicating octahedral geometry[35].

2.4 Magnetic property

The magnetic properties of complexes **1** and **2** were investigated over the temperature range of 2~300 K at an applied field of 1 000 Oe. As shown in Fig.8 (a), the $\chi_M T$ value of **1** at 300 K was 6.59 $cm^3 \cdot mol^{-1} \cdot K$, which is larger than the expected value of 3.75 $cm^3 \cdot mol^{-1} \cdot K$ for one isolated Co(Ⅱ) (S=3/2, g=2) ion[8]. As the temperature decreased, the value of $\chi_M T$ continuously decreased and reached a minimum value of 0.27 $cm^3 \cdot mol^{-1} \cdot K$ at 2 K. The data above 10~300 K fitted the Curie-Weiss law well with Curie constant C=7.08 $cm^3 \cdot mol^{-1} \cdot K$ and Weiss constant θ=−23.15 K (Fig.8(a)). The large negative θ value indicates dominant antiferromagnetic coupling[36-38]. For the Ni(Ⅱ) complex **2**, the $\chi_M T$ value at 300 K was 2.18 $cm^3 \cdot mol^{-1} \cdot K$, which is in agreement with the spin-only value of 2.0 $cm^3 \cdot mol^{-1} \cdot K$ for one isolated Ni(Ⅱ) (S=1/2, g=2.0) ion. Upon lowering the temperature, the $\chi_M T$ value decreased slowly until about 50 K, then decreased quickly to a minimum value of 0.47 $cm^3 \cdot mol^{-1} \cdot K$ at 2 K[8]. The data above 50~300 K fitted the Curie-Weiss law well with Curie constant C=2.19 $cm^3 \cdot mol^{-1} \cdot K$ and Weiss constant θ=−5.12 K (Fig.8(b)). The negative θ value and the decrease of $\chi_M T$ value suggest the dominant antiferromagnetic interactions above 50 K[36-38]. In **1** and **2**, two metal ions are connected by one μ_2-H_2O and two carboxylate group to form a magnetic exchange pathway of {⋯M-O-C-O-M⋯}.

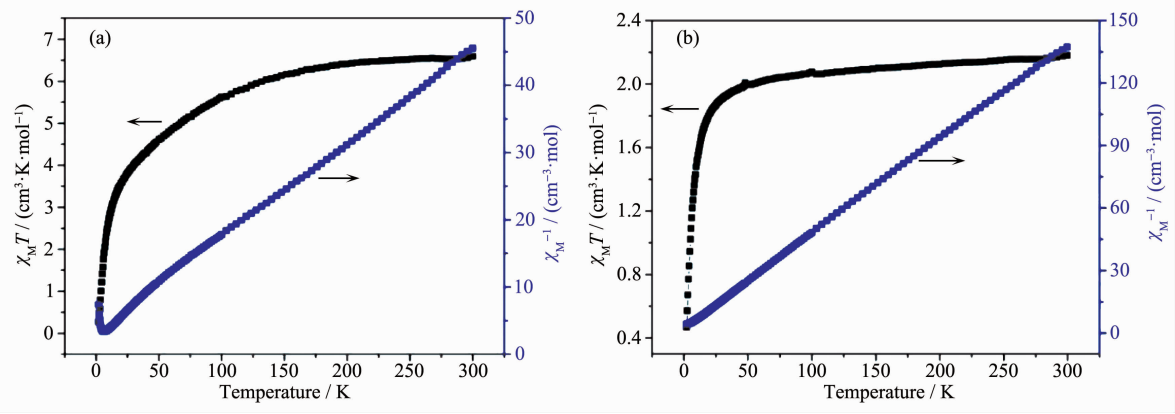

Fig.8　Temperature dependence of the $\chi_M T$ values for **1** (a) and **2** (b) at 1 000 Oe dc magnetic field

2.5 Catalytic capacity

As is known to all, the carbonyl compounds represent important applications in dyes, drugs and other fine chemicals. Inspired by unique advantages of metal organic frameworks materials[39], we decided to explore the catalytic performance of Co (Ⅱ)/Ni (Ⅱ) complexes in the oxidation of arylacycloalkane, and investigated the influence of central metals to catalytic behaviors. To expand the scope of complexes for oxidation of C-H bond, four substrates, including cyclanes and heterocyclic alkanes, were subjected to ketone under the optimized conditions (Table 2). It is obvious that the catalyst **1** behaved excellent catalytic performance, and the reason for this is Ni^{2+} is difficult to be completely oxidized to Ni^{3+} during the catalytic process. Proposed mechanism for the oxidation reaction indicated that there was a reversible oxidation/reduction transformation of central metal ions[28].

Table 2 Oxidation of arylacycloalkane catalyzed by Co(Ⅱ)/Ni(Ⅱ) complexes

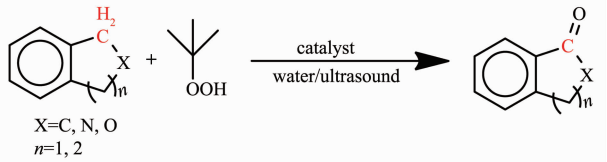

Entry	Catalyst	Substrate	Product	Yield / %
1	**1**	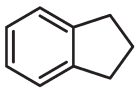	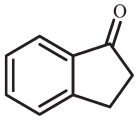	84
2	**2**			—
3	**1**	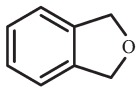	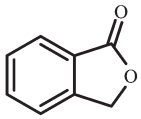	70
4	**2**			—
5	**1**	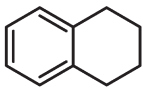	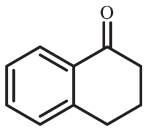	72
6	**2**			—
7	**1**	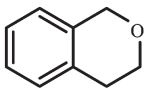	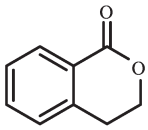	85
8	**2**			—

3 Conclusions

Two 3D complexes have been obtained by the coordination reactions of Co(Ⅱ)/Ni(Ⅱ) salts with 3,3′-(pyridine-3,5-diyl) dibenzoic acid (H_2pddb). Complexes **1** and **2** are isostructural, and H_2pddb ligands show same coordination modes. Magnetic studies for complexes **1** and **2** show an antiferromagnetic coupling between the adjacent Co(Ⅱ)/Ni(Ⅱ) centers. Furthermore, the catalyst **1** behaved excellent catalytic performance for the oxidation of arylacycloalkanes in aqueous medium.

Supporting information is available at http://www.wjhxxb.cn

References:

[1] Zhang J, Li B D, Wu X J, et al. *J. Mol. Struct.*, **2010**,**984**: 276-281

[2] Shen P P, Ren N, Zhang J J, et al. *J. Therm. Anal. Calorim.*, **2019**,**135**:2687-2695

[3] Fan Y R, Li H B, Jia Z Y, et al. *Inorg. Chem. Commun.*, **2019**,**102**:229-232

[4] Xing Y B, Liu Y Q, Meng B F, et al. *J. Chem. Crystallogr.*, **2019**:1-8

[5] Wu Y P, Xu G W, Dong W W, et al. *Inorg. Chem.*, **2017**,**56**: 1402-1411

[6] Ma K, Zhao Y N, Han X, et al. *Cryst. Growth Des.*, **2018**,**18**: 7419-7425

[7] Maity D K, Dey A, Ghosh S, et al. *Inorg. Chem.*, **2018**,**57**: 251-263

[8] Shao Z C, Han X, Liu Y Y, et al. *Dalton Trans.*, **2019**,**48**: 6191-6197

[9] Sun Y Y, Wang F, Zhang J. *Inorg. Chem.*, **2019**,**58**:4076-4079

[10]Zhao B, Li H J, Jia Y Y, et al. *Polyhedron*, **2014**,**68**:138-143

[11]WANG Gui-Xian(王桂仙), CAO Ke-Li(曹可利), CHEN Fei-Yan(陈飞燕), et al. *Chinese J. Inorg. Chem.*(无机化学学报), **2016**,**32**:43-48

[12]LIN Jian-Jun(林建军), LIU Zhen(刘珍), LÜ Ling-Zhi(吕灵芝), et al. *Chinese J. Inorg. Chem.*(无机化学学报), **2018**, **34**:230-236

[13]Zhao L, Zhang J, Wang J, et al. *J. Solid State Chem.*, **2018**, **268**:1-8

[14]Liu L, Huang C, Xue X, et al. *Cryst. Growth Des.*, **2015**,**15**: 4507-4517

[15]Corma A, García H, Xamena F X L I. *Chem. Rev.*, **2010**, **110**:4606-4655

[16]Yoon M, Srirambalaji R, Kim K. *Chem. Rev.*, **2012**,**112**: 1196-1231

[17]Zhao M, Ou S, Wu C D. *Acc. Chem. Res.*, **2014**,**47**:1199-1207

[18]Liu J, Chen L, Cui H, et al. *Chem. Soc. Rev.*, **2014**,**43**:6011-6061

[19]Dhakshinamoorthy A, Asiri A M, Garcia H. *Chem. Soc. Rev.*, **2015**,**44**:1922-1947

[20]Zhu Q L, Xu Q. *Chem. Soc. Rev.*, **2014**,**43**:5468-5512

[21]Wang H R, Meng W, Wu J, et al. *Coord. Chem. Rev.*, **2016**, **307**:130-146

[22]Park S S, Hontz E R, Sun L, et al. *J. Am. Chem. Soc.*, **2015**,**137**:1774-1777

[23]Chughtai A H, Ahmad N, Younus A Y, et al. *Chem. Soc. Rev.*, **2015**,**44**:6804-6849

[24]Yao H F, Yang Y, Liu H, et al. *J. Mol. Catal. A*: *Chem.*, **2014**,**394**:57-65

[25]Guo L, Huang C, Liu L, et al. *Cryst. Growth Des.*, **2016**,**16**: 4926-4933

[26]Shaabani A, Farhangi E, Rahmati A. *Appl. Catal. A*, **2008**, **338**:14-19

[27]Hossain M M, Shyu S. *Tetrahedron*, **2016**,**72**:4252-4257

[28]Gao K, Huang C, Yang Y, et al. *Cryst. Growth Des.*, **2019**, **19**:976-982

[29]*SAINT*, Bruker AXS, Inc., Madison, WI, **2001**.

[30]Sheldrick G M. *SADABS*, University of Göttingen, Germany, **2003**.

[31]Sheldrick G M. *Acta Crystallogr. Sect. A*: *Found. Crystallogr.*, **2008**,**A64**:112-122

[32]Liu P P, Wang C Y, Zhang M, et al. *Polyhedron*, **2017**,**129**: 133-140

[33]Zhou S B, Wang X F, Du C C, et al. *CrystEngComm*, **2017**, **19**:3124-3137

[34]Yan W, Han L J, Jia H L, et al. *Inorg. Chem.*, **2016**,**55**: 8816-8821

[35]Fan C, Zong Z, Zhang X, et al. *CrystEngComm*, **2018**,**20**: 4973-4988

[36]Li D S, Zhao J, Wu Y P, et al. *Inorg. Chem.*, **2013**,**52**:8091-8098

[37]Zeng M H, Zhou Y L, Wu M C, et al. *Inorg. Chem.*, **2010**, **49**:6436-6442

[38]Qin J, Jia Y, Li H, et al. *Inorg. Chem.*, **2014**,**53**:685-687

[39]Wang X, Liu M, Wang Y, et al. *Inorg. Chem.*, **2017**,**56**:13329-13336